SUPPLEMENTARY FIGURES

Figure S1

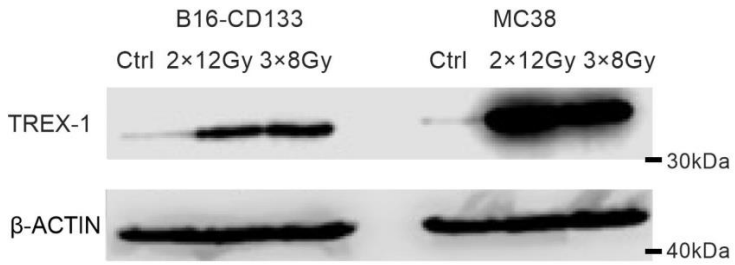

Figure S1: **hRT-induced expression of TREX1 in B16-CD133 melanoma cells and MC38 colon carcinoma cells**

The DNAse TREX1 was induced to a similar extent upon irradiation with 12 Gy × 2 or 8 Gy × 3 in both B16-CD133 melanoma cells and MC38 colon carcinoma cells 72h after the first irradiation.

Wang L, *et al. J Immunother Cancer* 2023; 11:e006235. doi: 10.1136/jitc-2022-006235

Figure S2

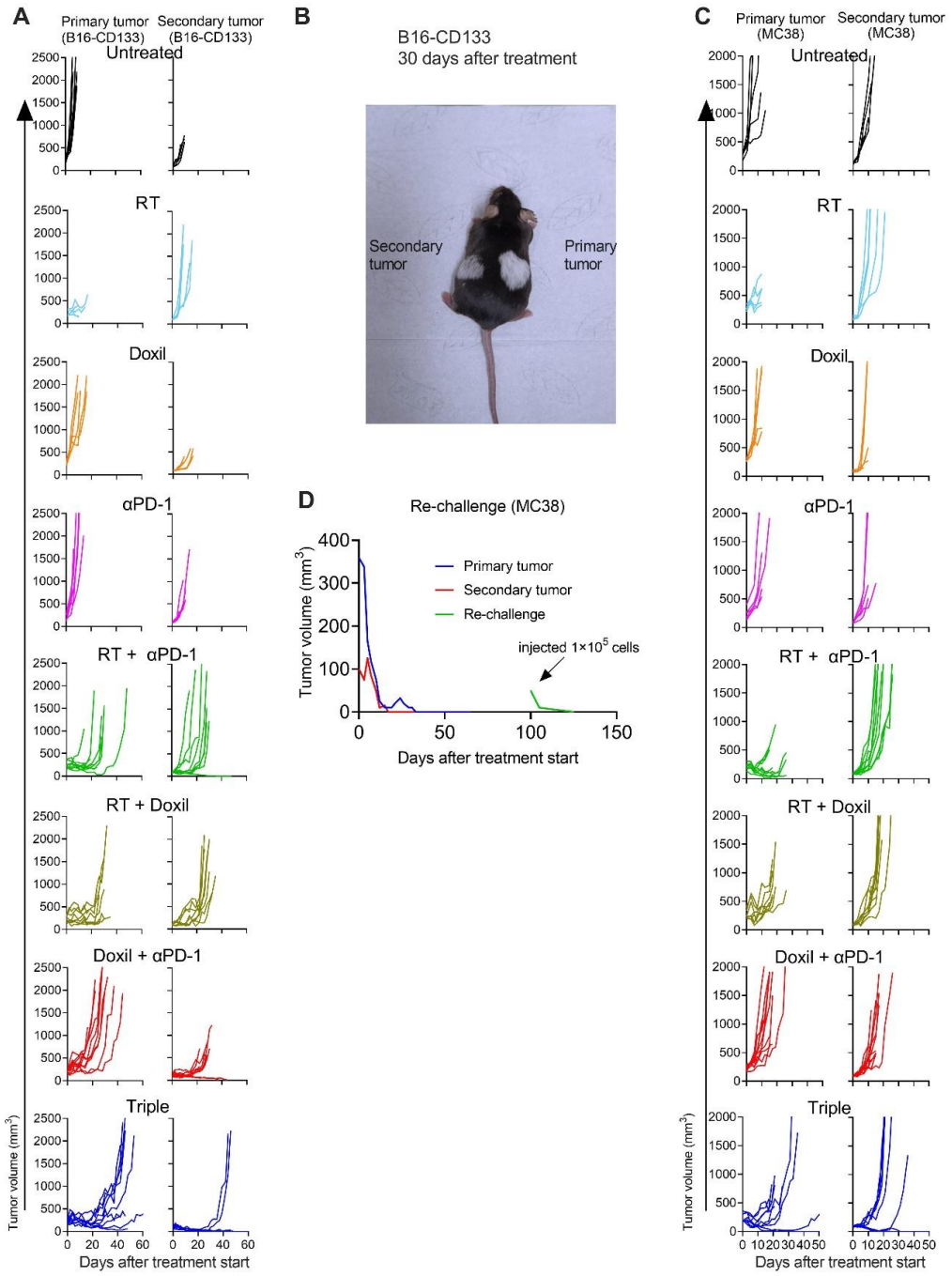

Figure S2. Adding Doxil to hRT and αPD-1 enhances the abscopal effect

Individual growth curves for B16-CD133 (**A**) and MC38 (**C**) tumors on the primary/irradiated and secondary/non-irradiated sites for the experimental groups shown in Fig. 1B and E. **B,**

Photo of a triple-treated mouse with a completely cured secondary and an almost completely cured primary B16-CD133 tumor 30 days after treatment start. **D,** MC38 abscopal model mouse cured by Doxil-containing triple therapy was re-challenged by injecting 1×10^5 live MC38 tumor cells 100 days after the cure.

Wang L, *et al. J Immunother Cancer* 2023; 11:e006235. doi: 10.1136/jitc-2022-006235

Figure S3

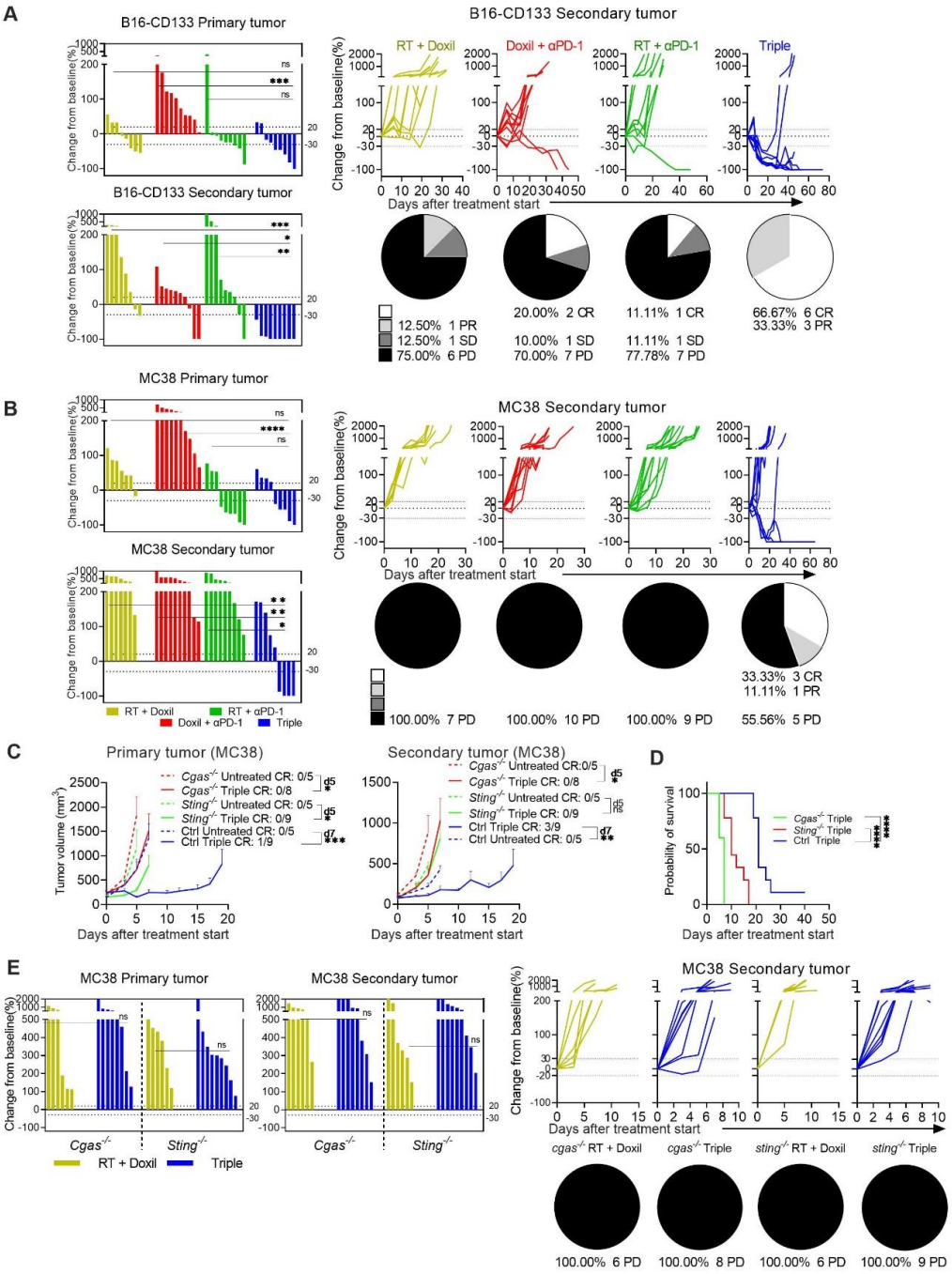

Figure S3. Waterfall and spider plots of tumor responses to treatment

(A) B16-CD133 and (**B**) MC38 tumor response (for the experiments shown in Fig. 1) assessed by % changes in tumor volume shown by waterfall and spider plots, and pie charts.

Wang L, *et al. J Immunother Cancer* 2023; 11:e006235. doi: 10.1136/jitc-2022-006235

Waterfall plots and pie charts are based on best relative changes in tumor volume that occurred from d10 after treatment start to the experimental endpoint, compared with treatment start. Waterfall plots show best response for each mouse. Pie charts show percentage of CR, PR, SD, and PD of the treatment groups according to modified RECIST1.1 as defined in Materials and Methods; ORR as given in the Results section equals CR + PR. Tumor growth (**C**) and survival curves (**D**) as well as waterfall plots, spider plots and pie charts (**E**) for experiments with mice bearing either *Cgas*$^{-/-}$ or *Sting*$^{-/-}$ or control nontargeted (*Cgas*$^{+/+}$*Sting*$^{+/+}$) MC38 tumor cells. In E, waterfall plots and pie charts show treatment response at d7 after tretment start. Data are presented as mean ± SEM. *P* values (ns, not significant; * $P < 0.05$; ** $P < 0.01$; *** $P < 0.001$; **** $P < 0.0001$) were determined by Kruskal-Wallis test with Dunn's test for multiple comparison correction (Waterfall plots in A, B and E), two-tailed t-test (C) and log-rank test (D). In C, the comparison time points for tumor volume measurement, i.e., the final time point at which no mouse of the compared groups had yet reached the experimental end point, are indicated.

Figure S4

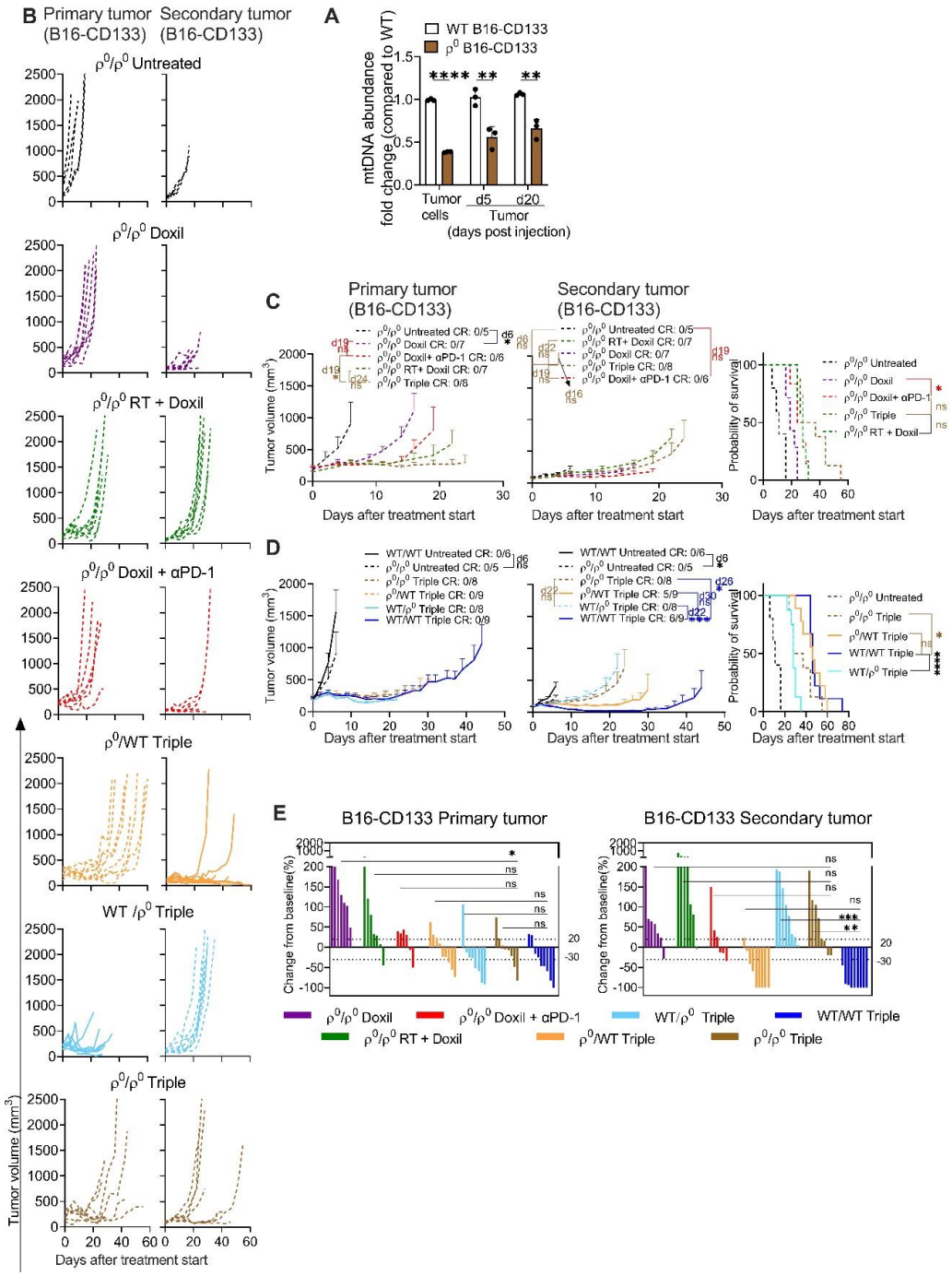

Figure S4. Importance of tumor cell mtDNA abundance for the Doxil-enhanced abscopal effect

Wang L, *et al. J Immunother Cancer* 2023; 11:e006235. doi: 10.1136/jitc-2022-006235

(A) mtDNA determined by qPCR in ddC-treated (ρ^0) or WT B16-CD133 cells and single-cell suspensions of tumors from ρ^0 or WT B16-CD133 cells. (**B)** Individual growth curves for B16-CD133 tumors for the experimental groups shown in Fig. 6B and S4C, D. (**C)** Tumor growth and survival curves of mice bearing bilateral tumors from mtDNA-depleted (ρ^0) B16-CD133 cells. (**D**) Tumor growth and survival curves of mice bearing bilateral B16-CD133 WT tumors, bilateral ρ^0 B16-CD133 tumors, or a ρ^0 tumor at the primary implantation site and a WT tumor at the secondary site. Dashed curves represent ρ^0 tumors. (**E**) Waterfall plots of best tumor response for each mouse between d10 after treatment start and endpoint, compared with treatment start. B, C and D, n = 5 - 9 mice per group. Data are presented as mean ± SEM. *P* values (ns, not significant; * $P < 0.05$; ** $P < 0.01$; *** $P < 0.001$; **** $P < 0.0001$) were determined by two-tailed t-test (A, C and D), log-rank test for survival analysis (C and D) and Kruskal-Wallis test with Dunn's test for multiple comparison correction (E). In C and D, the comparison time points for tumor volume measurement, i.e., the final time point at which no mouse of the compared groups had yet reached the experimental end point, are indicated.

Figure S5

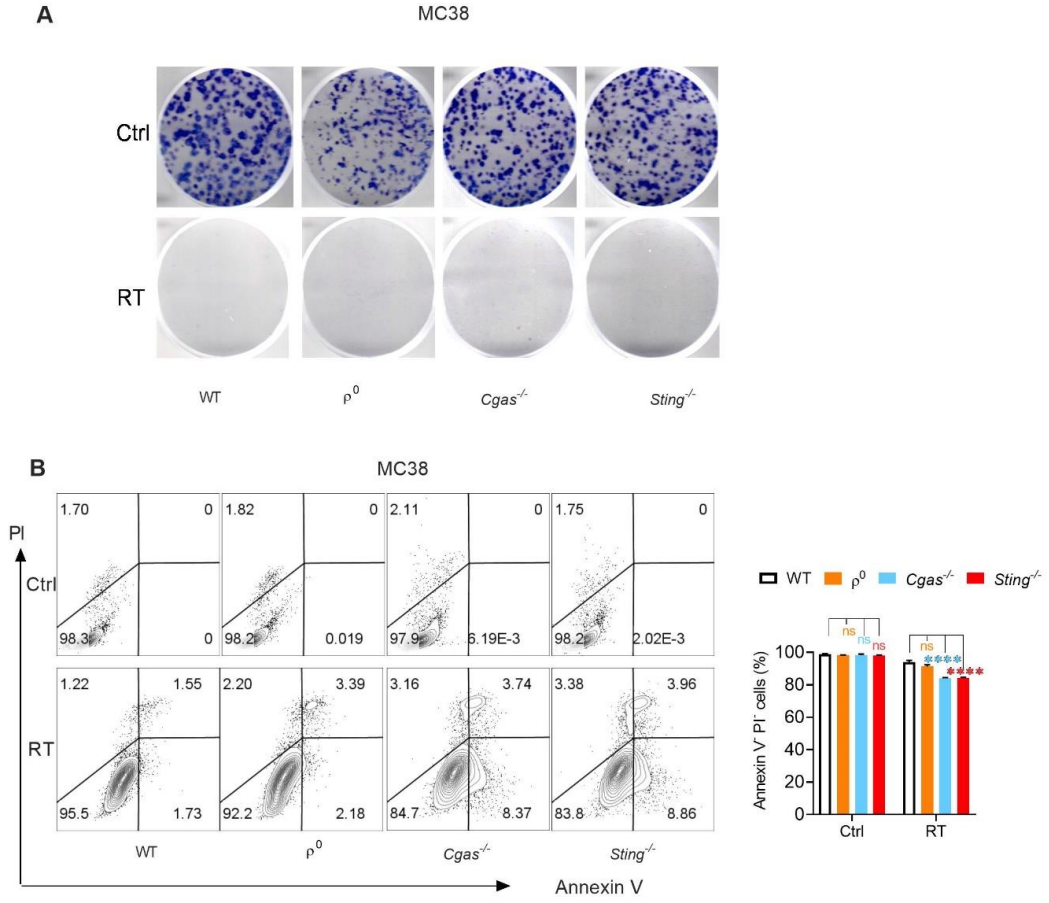

Figure S5: Apoptosis and clonogenic survival in irradiated MC38 colon carcinoma cells

Perturbing the cGAS/STING/mtDNA axis did not affect radiation-induced abrogation of clonogenic survival in MC38 cells (A), and it slightly enhanced apoptosis (16 h after irradiation) in Cgas-/- and in Sting-/- compared to WT tumor cells (B). The results shown are representative of two independent experiments with similar results. Gating for flow cytometry analysis was adjusted due to shifts in basis position of the irradiated compared to the unirradiated cells; this shift is most likely due to RT-induced changes in cell size.